Spin transport in as-grown and annealed thulium iron garnet/platinum bilayers with perpendicular magnetic anisotropy

Can Onur Avci, Andy Quindeau, Maxwell Mann, Chi-Feng Pai, Caroline A. Ross, and Geoffrey S. D. Beach

Phys. Rev. B **95**, 115428 — Published 24 March 2017

DOI: 10.1103/PhysRevB.95.115428

Spin transport in as-grown and annealed thulium iron garnet/platinum bilayers with perpendicular magnetic anisotropy

Can Onur Avci*, Andy Quindeau, Maxwell Mann, Chi-Feng Pai[1], Caroline A. Ross, Geoffrey S. D. Beach

Department of Materials Science and Engineering, Massachusetts Institute of Technology,

Cambridge, Massachusetts 02139, USA

**Email: canavci@mit.edu*

We characterize the spin Hall magnetoresistance (SMR), spin Seebeck effect (SSE) and damping-like spin-orbit torque (SOT) in thulium iron garnet/platinum bilayers with perpendicular magnetic anisotropy (PMA), by using harmonic Hall effect measurements. By consecutive annealing steps followed by measurements on a single device, we reveal that the spin-dependent effects gradually decrease in amplitude as the annealing temperature increases. We attribute this behavior primarily to the changes in the spin-mixing conductance which sensitively depends on the interface quality. However, further analysis demonstrates that, although the SSE scales closely with the SMR, the damping-like SOT shows a significantly different trend upon annealing, contrary to theoretical expectations. By comparing the damping-like SOT with the field-induced Hall effect we found evidence that scattering from Fe impurities in the Pt at the interface might be responsible for the distinct annealing temperature dependence of the damping-like SOT.

[1] Present address: Department of Materials Science and Engineering, National Taiwan University, Taipei 10617, Taiwan.

1. INTRODUCTION

Magnetic insulators (MIs) have emerged as an important material class due to their attractive magnetic properties that cannot be easily obtained in metallic magnetic materials. Ultralow damping, low saturation magnetization and large magnon decay lengths are some important attributes of certain types of MIs, particularly iron-based garnets.[1] Consequently MIs are highly efficient for generating, absorbing, and transmitting pure spin currents[2–4] providing the basis for future low-dissipation spintronic devices compatible with long-range spin transport and ultrahigh frequency operations.[5] Thus far, the majority of MI research has focused either on ferrites or on the archetypal yttrium iron garnet (YIG), due to its exceptional magnetic and optical properties.[1,6] By placing YIG in contact with a normal metal (NM) possessing large spin-orbit coupling (typically Pt) several interrelated spin transport phenemona have been revealed and studied by taking advantage of the direct and inverse spin Hall effects (SHE) in the NM that enable spin-charge interconversion.[3,4,7–10]

In particular, three spin-dependent effects have found broad interest in the spintronics community. The first one is the spin Hall magnetoresistance (SMR).[8,11–13] It describes the changes in the electrical resistivity of a non-magnetic metal (NM) adjacent to a MI depending on the magnetization orientation. As depicted in Fig. 1 (left panels), the effect arises due to the asymmetric scattering of the SHE-induced spin current at the MI/NM interface, which depends on the relative direction of the magnetization with respect to the spin polarization. The backscattered spin current contributes to the charge current via the inverse SHE, which ultimately manifests itself as a modification in the longitudinal and transverse resistivities.[14] A second widely-studied effect is spin-orbit torque (SOT).[15–19] SOTs are current-induced torques exerted on the magnetization as a result of strong spin-orbit coupling and inversion asymmetry. These SOTs typically originate from the SHE in the bulk of the NM (Fig.1 middle panels) and Rashba-Edelstein effect at the interfaces of dissimilar materials.[20–22] SOTs were first discovered and have been widely studied in all-metallic systems[18,23–27] whereas studies in MI/NM systems remain sparse.[28,29] This is mainly due to difficulties associated with the in-plane magnetization of most MIs and low electrical readout signal driven by SMR. However, recently, SMR and strong SOTs have been reported in a thulium iron garnet (TmIG)/Pt bilayer system possessing perpendicular magnetic anisotropy (PMA).[15,30] The PMA in this system was exploited to demonstrate current-induced

magnetization switching and direct electrical measurement of the damping-like SOT based on harmonic analysis of the SMR-driven Hall effect signal,[15,30] similar to all-metallic NM/ferromagnetic systems. Finally, the third prominent spin-dependent phenomenon is the spin Seebeck effect (SSE).[3,31–35] It describes pure spin current generation in a ferromagnetic material driven by a temperature gradient (∇T). The temperature difference along the gradient direction creates an imbalance in the magnon population which manifests itself as a spin current. This spin current, once it has diffused into a NM with large spin Hall angle, creates an inverse SHE or spin Seebeck voltage (V_{SSE}) as depicted in Fig.1 (right panels).

To generate and study the above spin-dependent effects, one requires: i) efficient spin transmission across the MI/NM interface, i.e. large and real spin mixing conductance ($G^{\uparrow\downarrow}$), ii) a spin Hall metal with appropriate properties such as large spin Hall angle and short spin diffusion length. The latter, being intrinsic material properties, cannot be easily modified. However the interface properties are more sensitive to sample preparation and post-growth processing, and play a major role in the measurement of the spin-dependent effects discussed above, i.e. the SMR, SOT and SSE. Therefore, altering the interface of a given system in a systematic manner can provide useful insight into the connections between these different effects and shed light on the underlying physics of these intriguing spin-dependent phenomena.

In this paper we report spin Hall magnetoresistance, spin Seebeck effect and damping-like SOT measurements in TmIG/Pt layers with perpendicular magnetic anisotropy. We quantitatively compare these measurements, performed on a single device, as a function of the thermal annealing temperature. The moderate annealing temperatures ($T_{ann} \leq 350°C$) used in this study are found to have a minor influence on the magnetic and electrical properties of TmIG and Pt, respectively, but have, in contrast, a large influence on the interface properties, namely the spin mixing conductance $G^{\uparrow\downarrow}$. Simultaneous analysis of the measured data reveals that the changes in the SMR and the SSE are relatively well correlated as a function of the annealing temperature whereas the damping-like SOT follows a significantly different trend. This result, which is contrary to theoretical expectations, suggests that additional contributions to damping-like SOT in this system are present. We present evidence that these contributions may be due to magnetic impurity scattering in the proximity of the TmIG/Pt interface. This result highlights the complex and intriguing physics behind the damping-like SOT

in MI/NM systems.

2. EXPERIMENTAL SETUP AND MEASUREMENT METHODS

a. Sample Preparation

To conduct the study, an 8-nm-thick $Tm_3Fe_5O_{12}$ (thulium iron garnet, TmIG) film was grown under tensile epitaxial strain on a (111)-oriented single crystal gadolinium gallium garnet substrate by pulsed laser deposition, followed by an ex-situ deposition of Pt (5nm) using DC magnetron sputtering. Due to its negative magnetostriction, the magnetoelastic anisotropy of TmIG exceeds the shape anisotropy (and magnetocrystalline anisotropy plays a minor role) leading to PMA with a magnetic easy axis in the out-of-plane [111] direction. More details about the sample preparation and characterization can be found in Refs.[15,30]. The continuous film was patterned into a Hall cross with dimensions of 8μm by 6μm [current line and Hall arm width, respectively, see Fig.2(a)] by using standard optical lithography and Ar^+ ion milling. Non-resonant harmonic Hall effect measurements were performed with a lock-in amplifier operated at 3678 Hz in a probe station where in-plane and out-of-plane magnetic fields can be applied simultaneously. Annealing of the device was performed in an inert Ar gas environment in the presence of an out-of-plane magnetic field of 4 kOe, with a dwell time of 1 h, ramped at 20 K/min. For the reference saturation magnetization (M_s) measurements a TmIG (20nm)/Pt (5nm) sample was prepared and annealed under nominally identical conditions and a vibrating sample magnetometer was used. All measurements were performed at room temperature.

b. Harmonic Hall Effect Measurements

Injecting an ac current with frequency ω into a Hall cross results in an oscillating Hall resistance with frequencies equal to multiples of ω, corresponding to first, second and higher order harmonics. The first harmonic resistance R_ω is equivalent to a standard Hall resistance (R_H) measured with a dc current, and probes the equilibrium magnetization- and field-driven signals which do not depend on the current itself. In the case of a MI/NM bilayer the first harmonic Hall resistance contains several contributions, mainly driven by the SMR, and expressed as follows:

$$\boldsymbol{R_\omega = R_H = R_{SMR}\sin^2\theta\sin 2\varphi + R_{AHE}\cos\theta + R_{OHE}H_z}. \quad (1)$$

Here R_{SMR}, R_{AHE} and R_{OHE} represent the transverse SMR, the SMR-induced anomalous Hall effect (AHE) resistance, and the ordinary Hall effect (OHE) resistance of the NM, respectively. H_z is the out-of-plane (OOP, **z**) component of the external field. The in-plane (IP) magnetization angle φ is defined in Fig. 2(a), whereas θ represents the magnetization angle with respect to the **z**-axis. According to the SMR theory based on a drift-diffusion model,[14] R_{SMR} and R_{AHE} are analogous to planar and anomalous Hall resistances in metallic ferromagnets, and attributed to the real ($\mathrm{Re}[\boldsymbol{G}^{\uparrow\downarrow}]$) and imaginary ($\mathrm{Im}[\boldsymbol{G}^{\uparrow\downarrow}]$) part of the interface spin mixing conductance, respectively, which itself sensitively depends on the interface. Typically in the MI/NM case $R_{SMR} \gg R_{AHE}$ when the interface allows an efficient spin transmission. We shall provide more details about these parameters in Sect. IIIc.

The second harmonic Hall effect signal contains information about the current-induced SOTs and thermally driven effects.[36] The appearance of the former is due to oscillations of the magnetization vector **m** around its equilibrium position mediated by the oscillating current-induced SOTs and Oersted field. The latter appears due to the quadratic dependence of the Joule heating on the injected current ($\propto I^2R$), which unavoidably establishes a temperature gradient (∇T) perpendicular to the layer plane due to preferential heat dissipation towards the substrate side.[37] Consequently, thermal voltages, corresponding predominantly to the anomalous Nernst effect and SSE, show up in the 2nd harmonic signal due to the dependence of ∇T on I^2, showing a symmetry of $V \propto \nabla\mathrm{T} \times \mathbf{m}$.[29,34,36,38] In the TmIG/Pt system the dominant thermally-driven signal is expected to be the SSE, as revealed by recent studies on similar MI/NM systems[39] since the anomalous Nernst effect requires the magnetic layer to be electrically conducting. We use the 2nd harmonic Hall resistance ($R_{2\omega}$) expression given in Ref.[18] where we replace the anomalous and planar Hall terms by the corresponding SMR-driven signals. By taking also into account the second harmonic resistance driven by the SSE, we can express $R_{2\omega}$ in TmIG/Pt as follows:

$$\boldsymbol{R_{2\omega} = (R_{AHE} - 2R_{SMR}\cos\theta\sin 2\varphi)\frac{d\cos\theta}{dH_{ext}}\frac{h_\theta}{\sin(\theta_H-\theta)} + 2R_{SMR}\sin^2\theta\cos 2\varphi\frac{h_\varphi}{H_{ext}\sin\theta_H} + R_{SSE}\sin\theta\cos\varphi}. \quad (2)$$

Here h_θ and h_φ are the polar and azimuthal components of the current-induced effective fields corresponding to SOTs and Oersted torque, θ_H is the polar angle of H_{ext}, and R_{SSE} is the 2nd harmonic resistance corresponding to the SSE.

We note that the SOTs consist of two components, damping-like ($\mathbf{T_{DL}}$) and field-like torque ($\mathbf{T_{FL}}$), and follow the symmetry below:[18,20]

$$\mathbf{T_{SOT}} \propto \mathbf{T_{DL}} + \mathbf{T_{FL}} = \boldsymbol{T_{DL}}\mathbf{m} \times (\mathbf{m} \times \mathbf{y}) + \boldsymbol{T_{FL}}\mathbf{m} \times \mathbf{y}, \quad (3)$$

where (T_{DL}, T_{FL}) are the scalar damping-like and field-like torque quantities, respectively, and $\mathbf{y}$ is the in-plane direction transverse to the current injection direction, as defined in Fig.2 (a). The corresponding effective fields are expressed as $\mathbf{H_{DL}} = \mathbf{T_{DL}} \times \mathbf{m}$ and $\mathbf{H_{FL}} = \mathbf{T_{FL}} \times \mathbf{m}$, with the Oersted field having the same symmetry as $\mathbf{H_{FL}}$. Finally, the scalar effective fields are expressed as $H_{\boldsymbol{DL}} \equiv \boldsymbol{T_{DL}}$ and $H_{FL} \equiv T_{FL}$.

3. RESULTS AND DISCUSSION

a. Annealing Temperature dependence of SMR and SMR-induced AHE

In order to measure the different SMR and OHE contributions given in Eq. 1, we measure R_H while sweeping the external field along OOP ($\theta_H = 0°$) and IP directions at ($\theta_H, \varphi_H = 90°, 45°$), respectively, in as-grown and annealed states. As depicted in Fig. 2(b), in the OOP field sweep (recorded at j_{rms}≈0.8x10^{11} A/m^2) we recognize two signal levels with sharp transitions corresponding to up ($\mathbf{m}_{up}$) and down ($\mathbf{m}_{down}$) state of the TmIG magnetization, and the difference is given by $R_{AHE} \times 2$. We also measure a non-negligible slope driven by R_{OHE} of Pt which is presumably independent of the material underneath, i.e. TmIG. The IP field sweep data exhibited in Fig. 2(c) show an U-shape behavior corresponding to coherent **m** rotation towards the plane upon increasing H_{IP}.This signal, mainly driven by R_{SMR}, follows a $\sin^2\theta$ symmetry [note that $\sin(2 \times 45°) = 1$], and saturates around H_{IP}~2 kOe when **m** fully aligns with the external field. We also observe a hysteretic region around $H_{IP} \cong 0$ with a smaller amplitude driven by R_{AHE}. This is due to slight unintentional misalignment of H_{IP} creating a small OOP component, which dictates the $\mathbf{m}_{up}$/$\mathbf{m}_{down}$ state in the absence of H_{IP}. We observe that thermal annealing creates substantial reduction in both R_{SMR} and R_{AHE}. We also note that these measurements are performed at a relatively higher current density ($j_{rms} = 2.5 \times 10^{11}$ A/m^2) to be

consistent with the 2nd harmonic measurements corresponding to SSE and SOT reported in the next section. Interestingly, we have found that R_{AHE} becomes larger (whereas R_{OHE} and R_{RHE} are nearly constant) upon increasing the current density. This suggests that the temperature rise due to Joule heating has a significant effect on R_{AHE}.

Next, we quantify R_{SMR} and R_{AHE} as a function of T_{ann} with the data shown in Fig. 2(c). We find that there is a linear relationship between these two quantities with no apparent offset, as illustrated in Fig.2(d). This remarkable correlation between R_{SMR} and R_{AHE} suggest that their driving mechanisms, believed to be $\mathrm{Re}[\boldsymbol{G}^{\uparrow\downarrow}]$ and $\mathrm{Im}[\boldsymbol{G}^{\uparrow\downarrow}]$, respectively, are affected in the same way by the physical changes taking place upon annealing.

To obtain more insight into the effect of annealing on the electrical and magnetic properties of the system we quantified the resistivity of Pt and the effective perpendicular anisotropy of TmIG [Fig. 2(f)]. We observe that the resistivity slightly decreases with increasing T_{ann}. This behavior, observed at moderate annealing temperatures, is attributed to the relaxation of the intrinsic tensile film stress in Pt which effectively increases the mean free path of electrons and thereby the conductivity.[40] We note that grain growth may also contribute. We also observe a slight decrease ($\sim 20\%$) in the effective perpendicular anisotropy field (H_K) which is given by the field required to entirely saturate **m** in-plane. However, VSM measurements on the reference TmIG/Pt sample show negligible variation in the saturation magnetization [see Fig.2 (f)] and coercivity upon annealing (not shown). This suggests that variations in H_K and *local* coercivity (region probed by the Hall cross, 6x8 μm^2) can result from the changes in the magnetic anisotropy energy, which is extremely sensitive to the strain state[30] and can slightly change upon moderate annealing. Therefore we conclude that the large variations in R_{SMR}, R_{AHE} and possibly the decrease in coercivity and H_K observed in Fig.2 (b,f) are predominantly due to the changes at the TmIG/Pt interface.

b. Annealing Temperature dependence of SSE and damping-like SOT

Now we focus on the $R_{2\omega}$ measurements to probe the SSE and SOTs. Typical measurement geometries to determine the SSE and SOTs are displayed in Fig. 3(a) and (b) upper panels, respectively. When **m** is tilted

along **x** [Fig. 3(a)], according to Eqs. 2 and 3, $h_\theta = H_{DL}$, $h_\varphi = H_{FL}$, and $R_{SSE} \neq 0$. On the other hand, when **m** is tilted perpendicular to **x** [Fig. 3(b)] $h_\theta = H_{FL}$ and $h_\varphi = H_{DL}$ and $R_{SSE} = 0$.

Figure 3(a) and (b) lower panels show the representative $R_{2\omega}$ signals (as-grown state) measured at a root-mean-square (RMS) current density of $j_{rms} = 2.5 \times 10^{11}$ A/m^2 in the field range of $|H_{IP}| \leq 4000$ Oe. We observe that $R_{2\omega}$ is much larger at $\varphi = 0°$ than at $\varphi = 90°$, and does not depend on H_{ext} above ≈ 1500 Oe. This is characteristic of a thermally-driven SSE signal, since SOT-originated signals should tend to zero at higher fields due to the reduced susceptibility of **m,** and hence reduced SOT-driven oscillations.[36] R_{SSE} is quantified by straightforward evaluation of the $R_{2\omega}$ amplitude in the lower panel of Fig. 3 (a) for all annealing temperatures. Measurement at $\varphi = 90°$ is considerably different and only shows a variation at fields lower than ≈ 1500 Oe. This signal is predominantly driven by SOTs because the SSE does not contribute to $R_{2\omega}$ in this geometry (see Eq. 2). Moreover we can neglect the first term on the right hand side of Eq. 2 which scales with R_{AHE}, since R_{SMR} is much larger than R_{AHE} [$R_{SMR}/R_{AHE} \cong 13.6$ as determined from the slope in Fig. 2(d)]. Consequently, the $R_{2\omega}$ signal at $\varphi = 90°$ mainly reflects the action of $h_\varphi = H_{DL}$. We plot $R_{2\omega}$ versus $2R_{SMR} \sin^2\theta / H_{ext}$ as suggested by Eq. 2 (notice that $\cos 2\varphi = \sin\theta_H = 1$) within the hysteretic region and find $H_{DL} = 18$ Oe by performing a linear fit [Fig. 3(c)]. We note that to accurately estimate $\sin^2\theta$ in the above given expression we performed an additional measurement at $\varphi = 45^\circ$ where $R_{SMR} \propto \sin^2\theta$ (not shown).

Based on the above analysis we plot R_{SSE} and H_{DL} as a function of T_{ann} in Fig. 4(a) and (b), respectively. Notice that the slight change in the device resistance upon annealing [see Fig. 2(e)] gives rise to different joule heating for the same applied current which is taken into account to normalize R_{SSE} values reported in Fig. 4(a). We observe that both effects reduce with the increasing T_{ann} but with different tendencies. We remark that R_{SSE} decreases rather linearly, reflecting approximately the changes in R_{SMR}. On the other hand H_{DL} is nearly constant up to $T_{ann} = 300°C$ and decreases abruptly upon annealing at $350°C$. These intriguing results call for a more detailed analysis which we perform in the following section.

c. Analysis and comparison of SMR, SSE and damping-like SOT

We find it sensible to examine the SMR, SSE and the damping-like SOT in terms of changes in $G^{\uparrow\downarrow}$ as a function of T_{ann} since this is presumably the most crucial parameter governing all three effects studied here. In order to estimate $\mathrm{Re}[G^{\uparrow\downarrow}]$ and $\mathrm{Im}[G^{\uparrow\downarrow}]$ we use the following expressions:[14]

$$\frac{\boldsymbol{R_{SMR}}}{\boldsymbol{R_{sq}}} = \boldsymbol{\theta_{SH}^2}\frac{\boldsymbol{\lambda_N}}{\boldsymbol{d_N}}\frac{\boldsymbol{2\lambda_N \mathrm{Re}[G^{\uparrow\downarrow}]\tanh^2\frac{d_N}{2\lambda_N}}}{\boldsymbol{\sigma_N + 2\lambda_N \mathrm{Re}[G^{\uparrow\downarrow}]\coth\frac{d_N}{\lambda_N}}}, \tag{4}$$

$$\frac{R_{AHE}}{R_{sq}} = \theta_{SH}^2\frac{\lambda_N}{d_N}\frac{2\lambda_N \mathrm{Im}[G^{\uparrow\downarrow}]\tanh^2\frac{d_N}{2\lambda_N}}{\sigma_N + 2\lambda_N \mathrm{Im}[G^{\uparrow\downarrow}]\coth\frac{d_N}{\lambda_N}}, \tag{5}$$

where θ_{SH}, λ_N, d_N, σ_N, and R_{sq} are the spin Hall angle, spin diffusion length, thickness, electrical conductivity and the square resistance of the NM, respectively. Additional to the directly accessible parameters such as d_N, σ_N, and R_{sq}, we need to estimate θ_{SH} and λ_N in order to accurately quantify $\mathrm{Re}[G^{\uparrow\downarrow}]$ and $\mathrm{Im}[G^{\uparrow\downarrow}]$. While we cannot evaluate λ_N with the present data we can determine θ_{SH} by assuming that H_{DL} is entirely driven by the SHE. To do this we insert the relevant material parameters into the expression[41] $\theta_{SH} = \frac{2e}{\hbar}\frac{M_s t_{Pt} H_{DL}}{j}$ and find $\theta_{SH} \approx 0.013$. This value is certainly an underestimation due to current spread in the Hall voltage arms that effectively reduces j in the central area of the Hall cross.[42] When this correction is taken into account we reassess $\theta_{SH} \sim 0.02 - 0.025,$ close to the reported values for Pt in contact with YIG but still lower than that of metallic Pt/ferromagnet bilayers.[43]

Next, we evaluate $\mathrm{Re}[G^{\uparrow\downarrow}]$ and $\mathrm{Im}[G^{\uparrow\downarrow}]$ based on Eqs. 4 and 5, by assuming that the measured R_{SMR} and R_{AHE} are entirely due to the SMR. We use $\theta_{\mathrm{SH}} = 0.025$ as determined above and $\lambda_N = 1.2$ nm, a commonly accepted value for Pt.[13] Fig. 5(a) exhibits $\mathrm{Re}[G^{\uparrow\downarrow}]$ and $\mathrm{Im}[G^{\uparrow\downarrow}]$ both of which decrease in the same way as T_{ann} is increased. Interestingly, we find very large values for $\mathrm{Re}[G^{\uparrow\downarrow}]$ (~10^{15} $\Omega^{-1}\mathrm{m}^{-2}$), comparable to the highest reported values for YIG/Pt.[7] However we caution that these results depend strongly on the choice of θ_{SH}. To highlight this point we have also calculated $G^{\uparrow\downarrow}$ by taking $\theta_{\mathrm{SH}} = 0.07$ (as typically assumed). The results are depicted in Fig. 5(b) where we find both $\mathrm{Re}[G^{\uparrow\downarrow}]$ and $\mathrm{Im}[G^{\uparrow\downarrow}]$ are more than one order of magnitude smaller. Nevertheless, independent of the parameter choice, these results suggest a rather efficient

transmission of the spin current through the TmIG/Pt interface, especially in the as-grown state, and degradation of the interface causes a gradual reduction in the spin transport efficiency.

To gain further insight into the T_{ann} dependence of the experimentally determined R_{SSE} and H_{DL} one must compare them with the SMR data on an equal footing. The amplitude of the electric field due to the inverse spin Hall effect in a NM resulting from spin pumping from an adjacent ferromagnet is well known (see e.g. Ref.[44]). Since the physics governing the spin dynamics at the interface and inside the NM should not depend on the manner by which spin current is generated inside the MI, we can adapt the expression originally developed for spin pumping in Ref.[44] and apply it to the spin Seebeck effect:

$$\boldsymbol{E_{SSE} = \theta_{SH} S_{SSE} \nabla T \frac{\lambda_N}{d_N} \frac{\mathrm{Re}[G^{\uparrow\downarrow}](1-\mathrm{sech}\frac{d_N}{\lambda_N})\coth\frac{d_N}{\lambda_N}}{\sigma_N+\lambda_N \mathrm{Re}[G^{\uparrow\downarrow}]\coth\frac{d_N}{\lambda_N}}} . \quad (6)$$

Here S_{SSE} is the spin Seebeck coefficient in units of V/m which incorporates a variety of material-dependent parameters such as the gyromagnetic ratio, saturation magnetization and magnetic coherence volume.[7] Similarly we use the damping-like torque expression developed in Ref.[20]:

$$\boldsymbol{T_{DL} = \theta_{SH}(1-\mathrm{sech}\frac{d_N}{\lambda_N}) \frac{|\tilde{G}|^2+\mathrm{Re}[\tilde{G}]\tanh^2\frac{d_N}{\lambda_N}}{|\tilde{G}|^2+2\mathrm{Re}[\tilde{G}]\tanh^2\frac{d_N}{\lambda_N}+\tanh^4\frac{d_N}{\lambda_N}}} , \quad (7)$$

where $\tilde{G}$ is the scaled spin mixing conductance and defined as $\tilde{G} = G^{\uparrow\downarrow}(2\lambda_N \tanh\frac{d_N}{\lambda_N}/\sigma_N)$. Now we can use Eqs. 6 and 7 to qualitatively estimate the $\mathrm{Re}[G^{\uparrow\downarrow}]$ dependence of R_{SSE} and H_{DL} in order to compare with the measured data. We note that the calculations are not exact since we are missing some material and experimental parameters such as S_{SSE} and ∇T but these are only scaling factors and presumably have negligible T_{ann} dependences. Therefore the calculated trends should be comparable to the experimental data. We consider two sets of $G^{\uparrow\downarrow}$, one estimated with $\theta_{\mathrm{SH}} = 0.025$ and the other with $\theta_{\mathrm{SH}} = 0.07$. Figure 6 shows the comparison between the experimental data (left axis) and calculations (right axis) for R_{SSE} (a,c) and H_{DL} (b,c). We find a notable difference between the theoretical estimation and the experimental data for both quantities, independent of the θ_{SH} choice. This implies that the SMR measurement does not agree with the SSE and H_{DL} measurements. It can be argued that, although there is no quantitative agreement, the trend for

the SSE is somewhat similar to the expectations. However the disagreement is substantial in the case of H_{DL}, which we find intriguing and further discuss below.

The unexpected T_{ann} dependency of H_{DL} can have several origins. One of the possible reasons could be a contribution of H_{FL} to the harmonic data, which is neglected in our analysis. In our previous work[15] we have performed simulations showing that H_{DL} can deviate from our reported value only by the ratio of R_{AHE}/R_{SMR}, i.e. 7%, if the two have comparable magnitudes. Although H_{FL} can have larger values with the increased T_{ann}, the changes would need to be unrealistically large to explain such an unexpected behavior. Moreover, if H_{FL} is very large, it cannot be the field-like component of the spin Hall torque, since it would scale with $\mathrm{Im}[G^{\uparrow\downarrow}]$,[20] which we find decreases with the same rate as $\mathrm{Re}[G^{\uparrow\downarrow}]$ upon annealing. Furthermore, if there is any H_{FL} present in the system, it should be much stronger than the Oersted field acting on TmIG by the current injection in Pt, since in the case of all-metallic structures these two were found to be opposite in sign. Another possible argument could be that R_{ω} and $R_{2\omega}$ signals are distorted due to an in-plane magnetic anisotropy giving rise to an incorrect estimation of H_{DL}. Detailed angle-dependent measurements on the same bilayer system (a different device) previously reported in Ref.[30] showed that, within our detection limit, the field required to saturate **m** fully in-plane is rather isotropic in the sample plane. This suggest that the in-plane magnetic anisotropy is negligible in this systems therefore its influence on the harmonic measurements can be neglected. Overall, these considerations strongly suggest that an incorrect estimation of H_{DL} cannot account for the observed behavior.

We realize that the T_{ann} dependency of H_{DL} follows a similar trend to that of R_{OHE} [determined by the measurements reported in Fig. 2(b)]. This correlation, illustrated in Fig. 7 is rather surprising since their driving mechanisms differ fundamentally. Indeed, we note that such strong variation in R_{OHE} is unexpected given that the changes in the bulk properties of Pt are too small to considerably modify the Lorentz force acting on conduction electrons. Recently, it has been reported that a significant paramagnetic-like signal contributes to the R_{OHE} in Pt/YIG, which sometimes even dominates based on Pt thickness and temperature. The paramagnetic Fe impurities in Pt, which are not coupled to the magnetization of YIG, in the vicinity of the interface were held responsible for the observation.[45,46] We can expect that the lighter atoms such as Fe

and O diffuse from TmIG towards Pt side during annealing, increasing the Fe impurity concentration in Pt close to the interface. It is likely that these impurities create a paramagnetic signal and modify the OHE slope which would be nearly constant for all T_{ann} otherwise. Unfortunately the maximum field that we can apply with our setup is too low to detect the signature of the paramagnetic signal which typically requires several T and follows approximately a Langevin function.[46] However, by tentatively attributing the changes in the R_{OHE} to the paramagnetic Hall effect contribution, thereby to the increased Fe impurity concentration, we speculate that additional (spin-dependent) scattering takes place, increasingly with T_{ann}, modifying the spin-torque properties driven by the SHE (i.e. H_{DL}) and consequently giving rise to the correlation observed in Fig. 4.

4. CONCLUSIONS

In conclusion, we have characterized the SMR, the Joule heating-induced SSE and the damping-like SOT in TmIG/Pt as a function of the thermal annealing temperature up to 350℃. Owing to the perpendicular magnetic anisotropy of TmIG we are able to accurately determine the above quantities based on harmonic Hall effect measurements. We find that in the as-grown state, the sample possesses a quite large spin mixing conductance ($\mathrm{Re}[G^{\uparrow\downarrow}] > 10^{15}$ $\Omega^{-1}\mathrm{m}^{-2}$) and a reasonable value of the spin Hall angle ($\theta_{\mathrm{SH}} \approx 0.025$). We further reveal that with increasing T_{ann}, the interface gradually degrades, and as a consequence, we observe a reduction in amplitude of all three spin-transport effects. We attribute this behavior primarily to the changes in the spin-mixing conductance which depends sensitively on the interface quality. However, further analysis demonstrates that with respect to the SMR the decrease of the SSE and especially the damping-like SOT shows a trend different to the theoretically predicted one. By comparing the damping-like SOT with the ordinary Hall effect, we found evidence that Fe impurities in Pt close to the interface might be responsible for the distinct annealing temperature dependence of the damping-like torque. This study reveals the complex dependence of the spin transport effects on the interface properties and calls for further investigation into their interdependence. Direct measurement of the spin-mixing conductance by an alternative method, such as ferromagnetic resonance, might be helpful to shed light on the observed annealing temperature dependence of the spin transport properties.

ACKNOWLEDGEMENTS

The authors would like to acknowledge support from C-SPIN, one of the six SRC STARnet Centers, sponsored by MARCO and DARPA. A.Q. acknowledges funding from the Deutsche Forschungsgemeinschaft (DFG, German Research Foundation) and from the Max-Planck-Institute of Microstructure Physics.

REFERENCES

[1] B.H. A. A. Serga, A. V. Chumak, J. Phys. D. Appl. Phys. **43**, 264002 (2010).

[2] B. Heinrich, C. Burrowes, E. Montoya, B. Kardasz, E. Girt, Y.Y. Song, Y. Sun, and M. Wu, Phys. Rev. Lett. **107**, 66604 (2011).

[3] K. Uchida, H. Adachi, T. Ota, H. Nakayama, S. Maekawa, and E. Saitoh, Appl. Phys. Lett. **97**, 172505 (2010).

[4] L.J. Cornelissen, J. Liu, R.A. Duine, J. Ben Youssef, and B.J. Van Wees, Nat. Phys. **11**, 1022 (2015).

[5] A.D. Karenowska, A. V. Chumak, A.A. Serga, and B. Hillebrands, Handb. Spintron. **11**, 1505 (2015).

[6] P. Hansen and J.P. Krumme, Thin Solid Films **114**, 69 (1984).

[7] M. Weiler, M. Althammer, M. Schreier, J. Lotze, M. Pernpeintner, S. Meyer, H. Huebl, R. Gross, A. Kamra, J. Xiao, Y.T. Chen, H. Jiao, G.E.W. Bauer, and S.T.B. Goennenwein, Phys. Rev. Lett. **111**, 176601 (2013).

[8] H. Nakayama, M. Althammer, Y.-T. Chen, K. Uchida, Y. Kajiwara, D. Kikuchi, T. Ohtani, S. Geprägs, M. Opel, S. Takahashi, and others, Phys. Rev. Lett. **110**, 206601 (2013).

[9] E. Villamor, M. Isasa, S. Vélez, A. Bedoya-Pinto, P. Vavassori, L.E. Hueso, F.S. Bergeret, and F. Casanova, Phys. Rev. B - Condens. Matter Mater. Phys. **91**, 020403(R) (2015).

[10] J.-C. Rojas-Sánchez, N. Reyren, P. Laczkowski, W. Savero, J.-P. Attané, C. Deranlot, M. Jamet, J.-M. George, L. Vila, and H. Jaffrès, Phys. Rev. Lett. **112**, 106602 (2014).

[11] N. Vlietstra, J. Shan, V. Castel, B.J. Van Wees, and J. Ben Youssef, Phys. Rev. B **87**, 184421 (2013).

[12] J. Kim, P. Sheng, S. Takahashi, S. Mitani, and M. Hayashi, Phys. Rev. Lett. **116**, 97201 (2016).

[13] C.O. Avci, K. Garello, A. Ghosh, M. Gabureac, S.F. Alvarado, and P. Gambardella, Nat. Phys. **11**, 570 (2015).

[14] Y.-T. Chen, S. Takahashi, H. Nakayama, M. Althammer, S. Goennenwein, E. Saitoh, and G. Bauer, Phys. Rev. B **87**, 144411 (2013).

[15] C.O. Avci, A. Quindeau, C.-F. Pai, M. Mann, L. Caretta, A.S. Tang, M.C. Onbasli, C.A. Ross, and G.S.D. Beach, Nat. Mater. DOI:10.1038/nmat4812 (2016).

[16] I.M. Miron, K. Garello, G. Gaudin, P.-J. Zermatten, M. V Costache, S. Auffret, S. Bandiera, B. Rodmacq, A. Schuhl, and P. Gambardella, Nature **476**, 189 (2011).

[17] L. Liu, C.-F. Pai, Y. Li, H.W. Tseng, D.C. Ralph, and R.A. Buhrman, Science (80-.). **336**, 555 (2012).

[18] K. Garello, I.M. Miron, C.O. Avci, F. Freimuth, Y. Mokrousov, S. Blügel, S. Auffret, O. Boulle, G. Gaudin, and P. Gambardella, Nat. Nanotech. **8**, 587 (2013).

[19] X. Qiu, P. Deorani, K. Narayanapillai, K.-S. Lee, K.-J. Lee, H.-W. Lee, and H. Yang, Sci. Rep. **4**, 4491 (2014).

[20] P.M. Haney, H.-W. Lee, K.-J. Lee, A. Manchon, and M.D. Stiles, Phys. Rev. B **87**, 174411 (2013).

[21] A. Brataas and K.M.D. Hals, Nat. Nanotech. **9**, 86 (2014).

[22] S. Emori, D.C. Bono, and G.S.D. Beach, Appl. Phys. Lett. **101**, 42405 (2012).

[23] C.O. Avci, K. Garello, C. Nistor, S. Godey, B. Ballesteros, A. Mugarza, A. Barla, M. Valvidares, E. Pellegrin, A. Ghosh, I.M. Miron, O. Boulle, S. Auffret, G. Gaudin, and P. Gambardella, Phys. Rev. B **89**, 214419 (2014).

[24] M. Jamali, K. Narayanapillai, X. Qiu, L.M. Loong, A. Manchon, and H. Yang, Phys. Rev. Lett. **111**, 246602 (2013).

[25] J. Kim, J. Sinha, M. Hayashi, M. Yamanouchi, S. Fukami, T. Suzuki, S. Mitani, and H. Ohno, Nat. Mater. **12**, 240 (2013).

[26] T.D. Skinner, M. Wang, A.T. Hindmarch, A.W. Rushforth, A.C. Irvine, D. Heiss, H. Kurebayashi, and A.J. Ferguson, Appl. Phys. Lett. **104**, 62401 (2014).

[27] X. Fan, H. Celik, J. Wu, C. Ni, K.-J. Lee, V.O. Lorenz, and J.Q. Xiao, Nat. Comm. **5**, 3042 (2014).

[28] A. Hamadeh, O. D'Allivy Kelly, C. Hahn, H. Meley, R. Bernard, A.H. Molpeceres, V. V. Naletov, M. Viret, A. Anane, V. Cros, S.O. Demokritov, J.L. Prieto, M. Muñoz, G. De Loubens, and O. Klein, Phys. Rev. Lett. **113**, 197203 (2014).

[29] N. Vlietstra, J. Shan, B.J. van Wees, M. Isasa, F. Casanova, and J. Ben Youssef, Phys. Rev. B **90**, 174436 (2014).

[30] A. Quindeau, C.O. Avci, W. Liu, C. Sun, M. Mann, A.S. Tang, M.C. Onbasli, D. Bono, P.M. Voyles, Y. Xu, J. Robinson, G.S.D. Beach, and C.A. Ross., Adv. Electron. Mater. **3**, 1600376 (2016).

[31] K. Uchida, S. Takahashi, K. Harii, J. Ieda, W. Koshibae, K. Ando, S. Maekawa, and E. Saitoh, Nature **455**, 778 (2008).

[32] D. Qu, S.Y. Huang, J. Hu, R. Wu, and C.L. Chien, Phys. Rev. Lett. **110**, 67206 (2013).

[33] C.M. Jaworski, R.C. Myers, E. Johnston-Halperin, and J.P. Heremans, Nature **487**, 210 (2012).

[34] M. Schreier, N. Roschewsky, E. Dobler, S. Meyer, H. Huebl, R. Gross, and S.T.B. Goennenwein, Appl. Phys. Lett. **103**, 242404 (2013).

[35] W.X. Wang, S.H. Wang, L.K. Zou, J.W. Cai, Z.G. Sun, and J.R. Sun, Appl. Phys. Lett. **105**, 182403 (2014).

[36] C.O. Avci, K. Garello, M. Gabureac, A. Ghosh, A. Fuhrer, S.F. Alvarado, and P. Gambardella, Phys. Rev. B **90**, 224427 (2014).

[37] H. Fangohr, D.S. Chernyshenko, M. Franchin, T. Fischbacher, and G. Meier, Phys. Rev. B **84**, 54437

(2011).

[38] C.O. Avci, K. Garello, J. Mendil, A. Ghosh, N. Blasakis, M. Gabureac, M. Trassin, M. Fiebig, and P. Gambardella, Appl. Phys. Lett. **107**, 192405 (2015).

[39] T. Kikkawa, K. Uchida, Y. Shiomi, Z. Qiu, D. Hou, D. Tian, H. Nakayama, X.-F. Jin, and E. Saitoh, Phys. Rev. Lett. **110**, 67207 (2013).

[40] U. Schmid and H. Seidel, J. Vac. Sci. Technol. **24**, 2139 (2006).

[41] L. Liu, O.J. Lee, T.J. Gudmundsen, D.C. Ralph, and R.A. Buhrman, Phys. Rev. Lett. **109**, 96602 (2012).

[42] I. Ibrahim, V. Schweigert, and F. Peeters, Phys. Rev. B **57**, 15416 (1998).

[43] M. Isasa, E. Villamor, L.E. Hueso, M. Gradhand, and F. Casanova, Phys. Rev. B **91**, 24402 (2015).

[44] V. Castel, N. Vlietstra, J. Ben Youssef, and B.J. Van Wees, Appl. Phys. Lett. **101**, 132414 (2012).

[45] Y. Shiomi, T. Ohtani, S. Iguchi, T. Sasaki, Z. Qiu, H. Nakayama, K. Uchida, and E. Saitoh, Appl. Phys. Lett. **104**, 2012 (2014).

[46] S. Shimizu, K.S. Takahashi, T. Hatano, M. Kawasaki, Y. Tokura, and Y. Iwasa, Phys. Rev. Lett. **111**, 216803 (2013).

FIGURES AND CAPTIONS

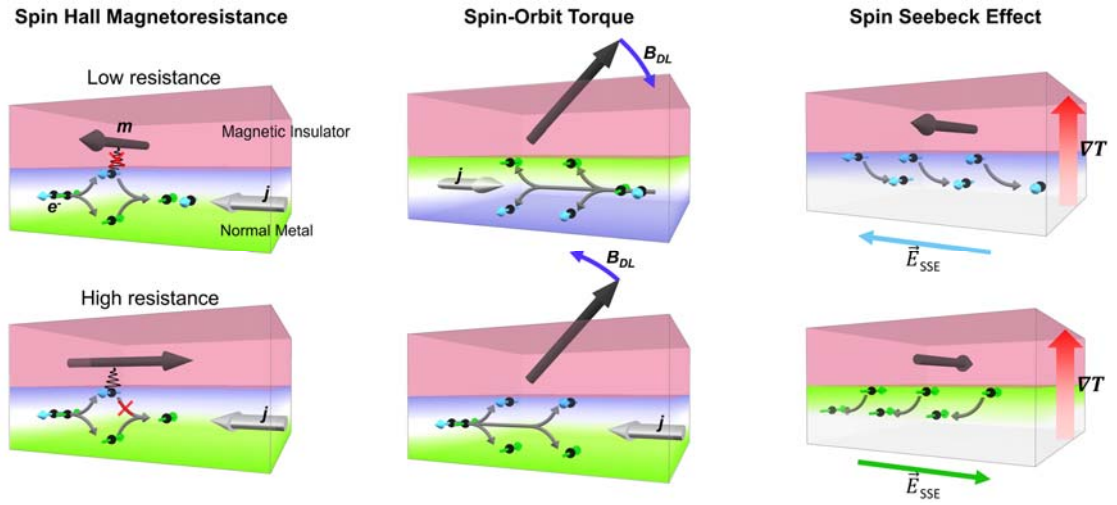

Figure 1 - Spin dependent effects in the MI/NM bilayer studied in this paper. Left panel shows the Spin Hall magnetoresistance. It is the change in the resistance of a normal metal in interfacial contact with a magnetic insulator depending on the magnetization orientation, which governs the SHE-induced spin current absorption/reflection at the interface. Middle panel shows the simplified damping-like spin-orbit torque mechanism driven by the spin Hall effect. The torque direction depends on the current injection direction due to reversal of the SHE-induced spin polarization at the MI/NM interface. Right panel shows the Spin Seebeck effect mechanism. A temperature gradient can generate a pure spin current in a magnetic material along the gradient direction, which can create a voltage across the NM due to the inverse SHE.

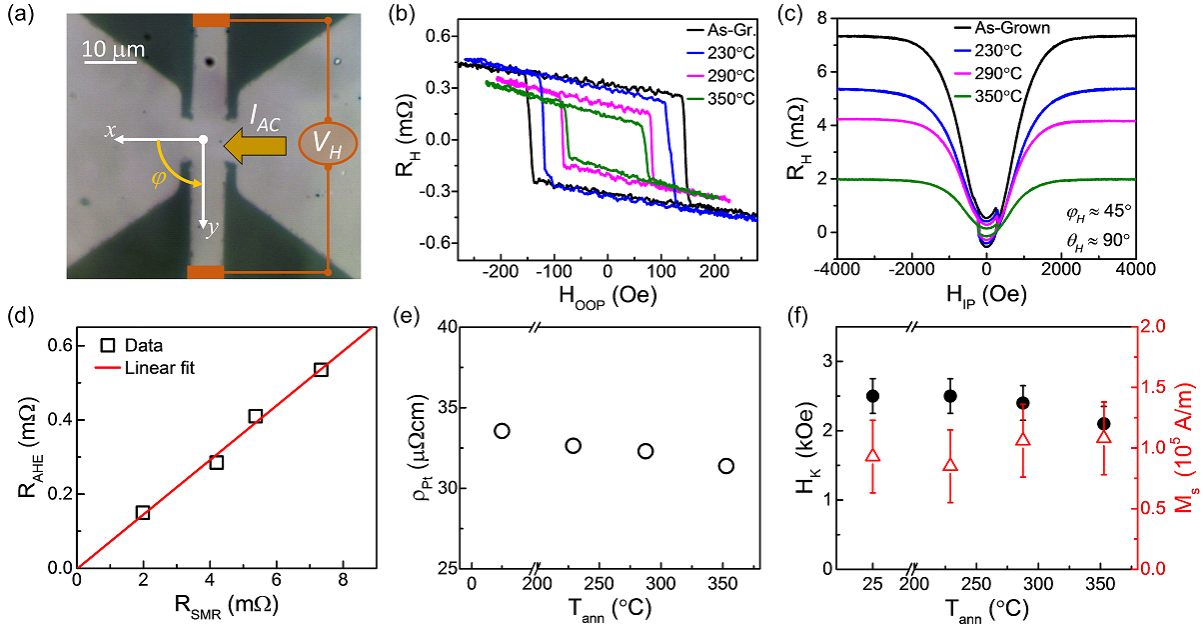

Figure 2 – (a) Optical microscopy image of the Hall cross device and the measurement scheme. Hall resistance with (b) OOP and (c) IP field sweeps for the as-grown and annealed sample. (d) SMR-driven anomalous Hall resistance vs. spin Hall magnetoresistance (red line is a linear fit to the data). (e) Electrical resistivity of Pt measured on the device as a function of annealing temperature. (f) left axis: Effective perpendicular anisotropy field determined by fitting the data

shown in (c) by macrospin simulations; right axis: saturation magnetization measured on reference TmIG(20nm)/Pt(5nm) bilayer.

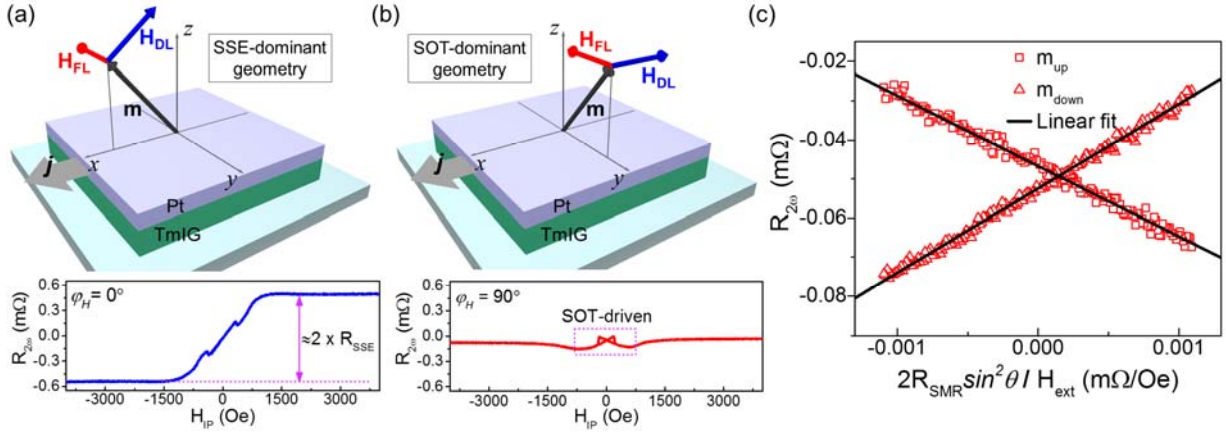

Figure 3 –Measurement scheme for the harmonic Hall effect measurements showing (a) SSE-dominant, (b) damping-like SOT-dominant geometry. Lower panels show the raw second harmonic signal taken in the as-grown state with an in-plane field sweep between ±3500 Oe. The current density is set to $j_{rms}=2.5x10^{11}$ A/m^2. (c) determination of the damping-like torque by fitting the second harmonic signal taken at (within the hysteretic region).

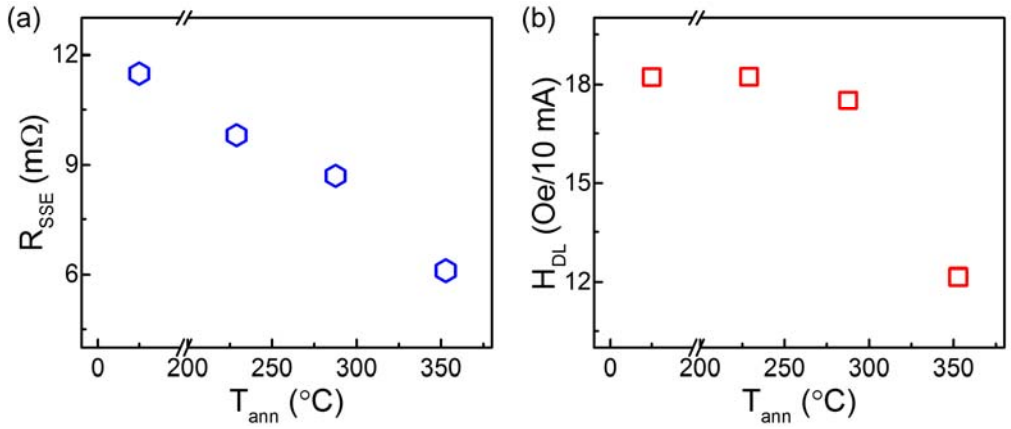

Figure 4 – (a) Spin Seebeck signal and (b) damping-like SOT as a function of annealing temperature.

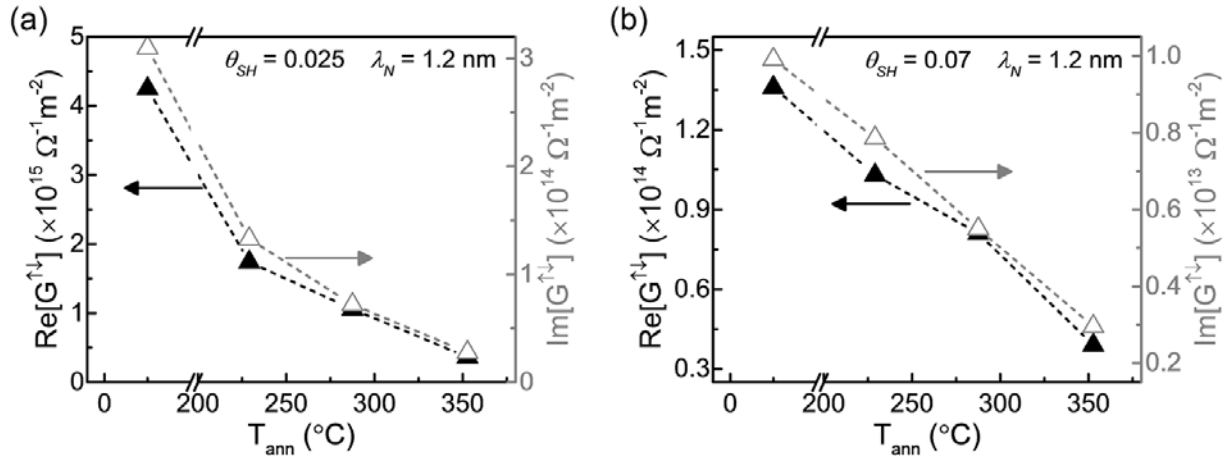

Figure 5 – Estimated spin mixing conductance as a function of annealing temperature, based on Eqs. 4 and 5, and two different sets of parameters for the spin Hall angle and spin diffusion length.

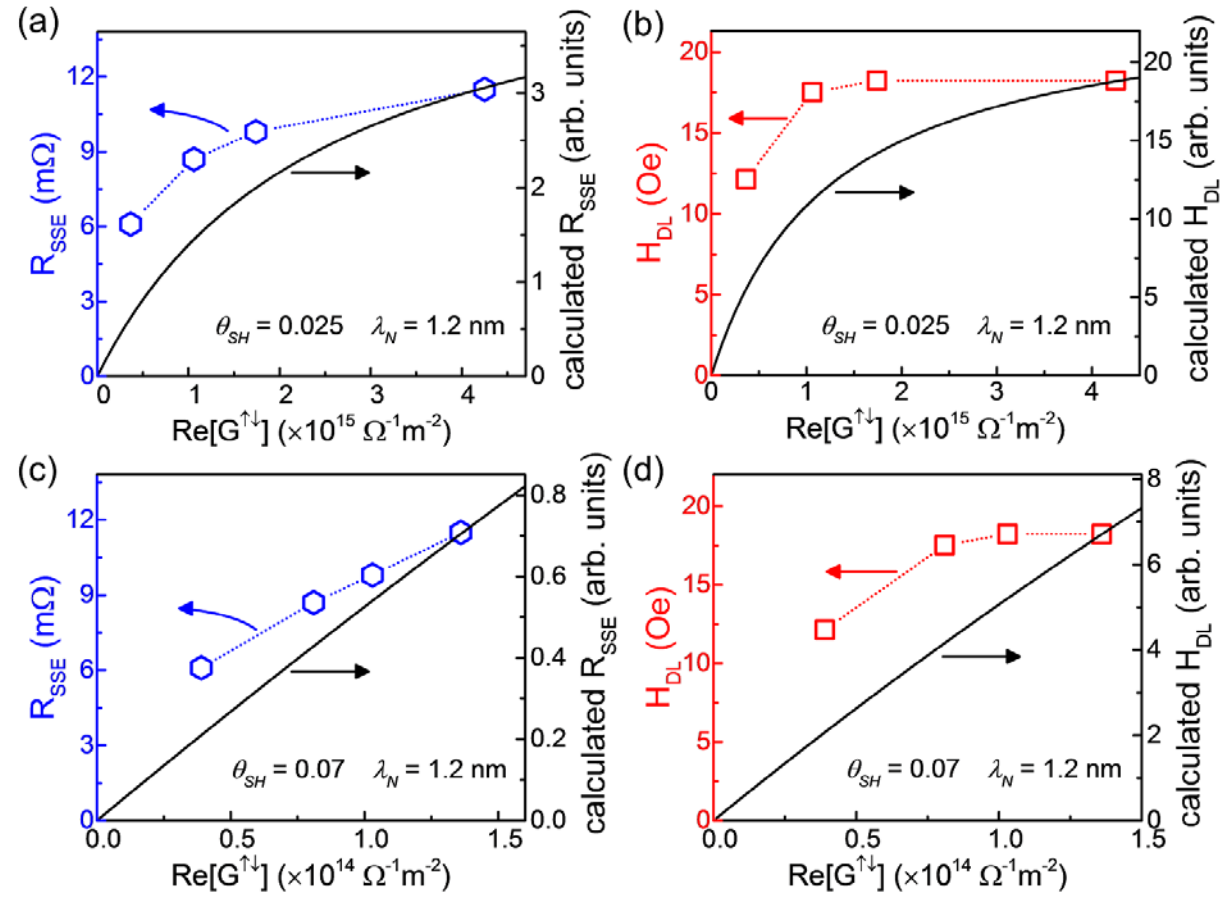

Figure 6 – Comparison of the measured SSE and damping-like SOT (left axis) with the theoretical estimations based on Eqs. 6 and 7. To estimate $Re[G^{\uparrow\downarrow}]$ the SMR expression given in Eq.4 is used. The y-axes have been chosen to match the rightmost data point corresponding to the as-grown state.

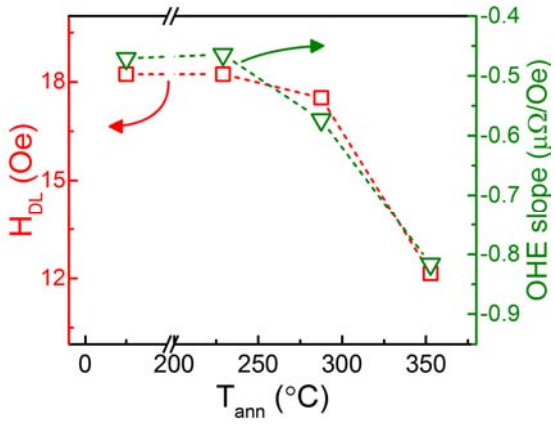

Figure 7 – Damping-like SOT (left axis) and the ordinary Hall effect slope (right axis) versus the annealing temperature. There is an apparent correlation between these two quantities.